J Geophys (1985) 58:146–152

Journal of Geophysics

The reflectivity method for different source and receiver structures and comparison with GRF data

R. Kind

Seismologisches Zentralobservatorium, Krankenhausstrasse 1, 8520 Erlangen, Federal Republic of Germany

Abstract. A brief review of the reflectivity method is given, including a new analytical solution of the layer matrix equation. The method is extended to allow the computation of complete body waves for different source and receiver structures. Applications of theoretical seismograms to the Gräfenberg broadband data are shown. Examples are the detection of depth phases at regional distances in southern Germany, which leads to improved source depth determinations, and the computation of the complete *P*-wave group for events in ocean-covered areas.

Key words: Reflectivity method – Lateral inhomogeneities – Regional broadband seismograms

Introduction

The reflectivity method is one of the major methods for the computation of theoretical seismograms. It is a simple-to-use and a complete method for computing the effects of the earth structure on propagating elastic waves. The large number of applications range from deep seismic sounding studies to studies of the inner core, and from surface – wave studies to studies of the structure-source interference. The method was invented at the end of the 1960s and it has been continuously developed and used since then. Limitations of the method are its long computation times and the restriction to laterally homogeneous models. In this paper the method will be extended to a special case of lateral inhomogeneities.

The reflectivity method is based on the Haskell matrix formalism for the propagation of plane waves through plane-layered media. The transformation from monochromatic plane waves into impulsive spherical waves due to a point source is carried out by a double numerical integration over frequency and wavenumber. The question of the appropriate sampling interval in the frequency-wavenumber domain and the associated aliasing problems are very important. From a practical point of view, the use of complex frequencies has solved the aliasing problem in the time domain (Phinney, 1965). In the distance domain this problem was solved by a transformation of the variables from wavenumber to angle of incidence (in the original formulation of the method) or slowness. The slowness integration is carried out along the real axis: poles of the integrand are shifted away using attenuation via complex frequencies (Schwab and Knopoff, 1972). Problems in the numerical evaluation of the layer matrices have existed for a long time. But continuous analytical and numerical improvements have essentially solved this problem. Kennett (1983) has developed an algorithm which is an analytical solution. Kind and Odom (1983) use a numerical solution. Spherical earth models are computed using an earth flattening approximation.

The method was developed by Fuchs (1968). Fuchs and Müller (1971) formulated a version which is widely used in deep seismic sounding and studies of the deeper structure of the earth. Kind (1978, 1979a) developed a version of this method for the computation of complete earthquake seismograms.

Solution of the layer matrix equation

We consider a stack of homogeneous flat layers with a free surface on top and a half-space at the bottom. One of the layers contains a source. A detailed description of this case may be found in Harkrider (1964). The results is a matrix equation which relates the displacements and stresses at an arbitrary depth to the model and source parameters. A solution for the desired displacements of this equation seems trivial. But the problem is to find an analytical solution which is suitable for the numerical computations.

The Haskell matrix **A** is defined as a function which carries the displacements and stresses from one interface to the next. In the case of many layers, the product of the Haskell matrices does the same. Therefore, we have

$$\mathbf{T}_k^+ = \mathbf{A} * \mathbf{T}_0 \tag{1}$$

where $\mathbf{T}_k^+$ is, for example, the displacement-stress vector just above an arbitrary interface k and $\mathbf{T}_0$ is the same at the free surface. In this case we define $\mathbf{T}_k^+ = (W, X, Y, Z)^+$ and $\mathbf{T}_0 = (u, w, 0, 0)$ with $\mathbf{A} = a_{ij}$ $(i, j = 1, 2, 3, 4)$. The u and w are the radial and vertical displacement components at the free surface. The stress components are zero at the free surface. Equation (1) now becomes

$$\begin{pmatrix} W \\ X \\ Y \\ Z \end{pmatrix}^{+} = \mathbf{A} * \begin{pmatrix} u \\ w \\ 0 \\ 0 \end{pmatrix}$$

or

$$\begin{pmatrix} W \\ X \end{pmatrix}^{+} = \mathbf{A}_1 * \mathbf{A}_2^{-1} * \begin{pmatrix} \mathbf{Y} \\ \mathbf{Z} \end{pmatrix}^{+}$$

with

$$\mathbf{A}_1 = \begin{pmatrix} a_{11} & a_{12} \\ a_{21} & a_{22} \end{pmatrix}, \quad \mathbf{A}_2 = \begin{pmatrix} a_{31} & a_{32} \\ a_{41} & a_{42} \end{pmatrix},$$

$$\mathbf{A}_2^{-1} = \begin{pmatrix} a_{42} & -a_{32} \\ -a_{41} & a_{31} \end{pmatrix} / \det(\mathbf{A}_2).$$

The product $\mathbf{A}_1 * \mathbf{A}_2^{-1}$ leads directly to the delta matrices. We define

$$a_{m2} * a_{n1} - a_{m1} * a_{n2} = a \begin{pmatrix} m & n \\ 2 & 1 \end{pmatrix} = R_{i1}$$

where $i = 1, 2, 3, 4, 5, 6$ corresponds to the index pair $mn = 21, 31, 41, 32, 42, 43$. A description of the delta matrices may be found in Zurmühl (1964). Delta matrices were introduced into seismology by Dunkin (1965). Their elements consist of 2×2 sub-determinants of the Haskell matrix. The main advantage of their use is that they avoid unnecessary operations with very large or very small numbers.

The R_{i1} are the delta matrix elements. Now we have the relation

$$\begin{pmatrix} W \\ X \end{pmatrix}^{+} = \mathbf{Q} * \begin{pmatrix} Y \\ Z \end{pmatrix}^{+} \tag{2}$$

with $Q_{11} = R_{31}/R_{61}$, $Q_{12} = -R_{21}/R_{61}$, $Q_{21} = R_{51}/R_{61}$, $Q_{22} = -R_{41}/R_{61}$. Equation (2) relates the two displacement components at an arbitrary interface to the two stress components at the same interface, for the case of an arbitrary stack of plane layers with a free surface on top. The function that carries out this relation contains five elements of the first column of the product delta matrix of all considered layers.

Next we consider $\mathbf{T}_k^-$, the displacement-stress vector just below the interface k. This vector is related to $\mathbf{T}_n$, the same vector at the interface of the half-space, by $\mathbf{T}_n = \mathbf{B} * \mathbf{T}_k^-$. The matrix $\mathbf{B}$ is the product Haskell matrix of all layers between the interfaces n and k. We impose the condition of no radiation from the half-space back into the layered medium. For this purpose we must split the displacements and stresses into their up- and down-going potentials. The relations between potentials and displacements and stresses may also be found in Harkrider (1964). This relation is

$$\mathbf{E} * \begin{pmatrix} P_d + P_u \\ P_d - P_u \\ S_d - S_u \\ S_d + S_u \end{pmatrix} = \mathbf{T}_n.$$

P_u, P_d, S_u and S_d are the up- and down-going potentials for P and S waves, respectively. We require no up-going waves in the half-space, therefore we set $P_u = S_u = 0$. It follows that

$$\begin{pmatrix} P_d \\ P_d \\ S_d \\ S_d \end{pmatrix} = \mathbf{E}_n^{-1} * \mathbf{B} * \begin{pmatrix} W \\ X \\ Y \\ Z \end{pmatrix}^{-}. \tag{3}$$

Taking the differences between line 1 and line 2, and between line 3 and line 4 in Eq. (3), gives

$$\begin{pmatrix} 0 \\ 0 \end{pmatrix} = \mathbf{D} * \begin{pmatrix} W \\ X \\ Y \\ Z \end{pmatrix}^{-}.$$

Here $\mathbf{D}$ is the two-lines and four-columns difference matrix of $\mathbf{E}_n^{-1}$ multiplied with $\mathbf{B}$. In the same manner as above we write

$$\begin{pmatrix} W \\ X \end{pmatrix}^{-} = \mathbf{D}_1^{-1} * \mathbf{D}_2 * \begin{pmatrix} Y \\ Z \end{pmatrix}^{-},$$

with

$$\mathbf{D}_1 = \begin{pmatrix} d_{11} & d_{12} \\ d_{21} & d_{22} \end{pmatrix}, \quad \mathbf{D}_2 = \begin{pmatrix} d_{13} & d_{14} \\ d_{23} & d_{24} \end{pmatrix},$$

$$\mathbf{D}_1^{-1} = \begin{pmatrix} d_{22} & -d_{12} \\ -d_{21} & d_{11} \end{pmatrix} / \det(\mathbf{D}_1).$$

The product $\mathbf{D}_1^{-1} * \mathbf{D}_2$ again leads directly to the delta matrices. We define

$$d_{1m} * d_{2n} - d_{1n} * d_{2m} = d \begin{pmatrix} 1 & 2 \\ m & n \end{pmatrix} = S_{1i},$$

with the same correspondence of the indices as above. The S_{1i} are the delta matrix elements. Now we obtain

$$\begin{pmatrix} W \\ X \end{pmatrix}^{-} = \mathbf{C} * \begin{pmatrix} Y \\ Z \end{pmatrix}^{-}, \tag{4}$$

with $C_{11} = S_{14}/S_{11}$, $C_{12} = S_{15}/S_{11}$, $C_{21} = -S_{12}/S_{11}$, $C_{22} = -S_{13}/S_{11}$. Equation (4) relates the two displacement components at an arbitrary interface to the two stress components at the same interface, under the condition that there exists an arbitrary stack of plane layers with an underlying half-space, and if there is no radiation from the half-space into the layers. The function that carries out this relation contains five elements of the first line of the product delta matrix of all layers considered. Note that the third and fourth element in the first line are equal.

We introduce the source now, as follows:

$$\mathbf{T}_k^{-} = \mathbf{T}_k^{+} + \mathbf{S}. \tag{5.}$$

Here, the displacement-stress vector $\mathbf{S}$ describes the source. In the absence of a source, the displacements and stresses at each interface are continuous. The displacements and stresses at the interface k in Eq. (5) may be computed using the relations (2) and (4). If we want to compute the displacements at the free surface, in the

half-space or anywhere else in the model, we must compute the Haskell matrix of all layers between k and our desired interface. Then the displacements and stresses at k are multiplied with this matrix (if the desired interface is below k) or its inverse (if the desired interface is above k).

The reflectivity method for different source and receiver structures

The computation of theoretical seismograms for this case was treated earlier by Kennett (1975), but he did not compute the complete response of the source and the receiver structures. More recently, Chang-Eob Baag and Langston (1985) treated the case for the complete SV response of the source and receiver structure. The purpose of this extension is to compute the full P-SV response of the structure in which the earthquake occurs, to carry this response in full through the mantle and, finally, to compute the full response of the receiver structure. The full response of each of the three parts of the model will be computed. But the response will not be complete for the entire model, since not all the possible waves are computed at the interface where the individual parts of the entire model are connected.

The first step is to compute the down-going P- and S-wave potentials at the source side. For this purpose we compute first the displacement and stresses at the source interface k in Eq. (5), using Eqs. (2) and (4). From Eq. (5) it follows that

$$\begin{pmatrix} W \\ X \end{pmatrix}^- = \begin{pmatrix} W \\ X \end{pmatrix}^+ + \begin{pmatrix} S_1 \\ S_2 \end{pmatrix},$$

$$\begin{pmatrix} Y \\ Z \end{pmatrix}^- = \begin{pmatrix} Y \\ Z \end{pmatrix}^+ + \begin{pmatrix} S_3 \\ S_4 \end{pmatrix}$$

with $\mathbf{S}=(S_1, S_2, S_3, S_4)$. Now Eqs. (2) and (4) are applied to the first of these equations

$$\mathbf{C}\begin{pmatrix} Y \\ Z \end{pmatrix}^- = \mathbf{Q}\begin{pmatrix} Y \\ Z \end{pmatrix}^+ + \begin{pmatrix} S_1 \\ S_2 \end{pmatrix},$$

and we replace $(Y, Z)^+$:

$$\mathbf{C}\begin{pmatrix} Y \\ Z \end{pmatrix}^- = \mathbf{Q}\left[\begin{pmatrix} Y \\ Z \end{pmatrix}^- - \begin{pmatrix} S_3 \\ S_4 \end{pmatrix}\right] + \begin{pmatrix} S_1 \\ S_2 \end{pmatrix}.$$

From this it follows that

$$\begin{pmatrix} Y \\ Z \end{pmatrix}^- = (\mathbf{C}-\mathbf{Q})^{-1} * \left[-\mathbf{Q}\begin{pmatrix} S_3 \\ S_4 \end{pmatrix} + \begin{pmatrix} S_1 \\ S_2 \end{pmatrix}\right]. \tag{6}$$

Equation (4) is now used to compute $(W, X)^-$, and with this the displacements and stresses at the source interface k are known. These results are used to compute the down-going potentials P_d and S_d in Eq. (3).

The next step is to use P_d and S_d just obtained as input for the mantle structure and to compute the reflected potentials P_u and S_u. From the relation between the potentials and the displacement-stress vector, it follows that

$$\begin{pmatrix} P_d+P_u \\ P_d-P_u \\ S_d-S_u \\ S_d+S_u \end{pmatrix} = \mathbf{E}_n^{-1}\begin{pmatrix} W \\ X \\ Y \\ Z \end{pmatrix}. \tag{7}$$

The index n is, at the same time, the index of the half-space at the top of the mantle and the index of the half-space below the source crust. Therefore, it is convenient to introduce a non-physical boundary between source structure and mantle, with no contrast in material properties across this boundary. We sum the first and the last two lines of Eq. (7) and get

$$\begin{pmatrix} 2P_d \\ 2S_d \end{pmatrix} = \mathbf{S}_1\begin{pmatrix} W \\ X \end{pmatrix} + \mathbf{S}_2\begin{pmatrix} Y \\ Z \end{pmatrix},$$

where $\mathbf{S}_1$ contains the first four elements of the summation matrix of $\mathbf{E}_n^{-1}$, and $\mathbf{S}_2$ contains the last four elements of that matrix. Now we apply Eq. (4) to the mantle model. Recall that it was derived for the case of a layered half-space below the interface and no radiation into the half-space from infinity. It follows that

$$\begin{pmatrix} 2P_d \\ 2S_d \end{pmatrix} = (\mathbf{S}_1 * \mathbf{C} + \mathbf{S}_2) * \begin{pmatrix} Y \\ Z \end{pmatrix}.$$

This equation, together with Eq. (4), can be used to compute all components of the displacement-stress vector at the top of the mantle. Equation (7) now contains all necessary known quantities, and P_u and S_u can be computed directly.

The last step is to carry the obtained up-going potentials through the receiver model to the free surface, where the observer is located. We start from Eq. (7) and use the Haskell matrix $\mathbf{A}$ of the receiver model to carry the vector (W, X, Y, Z) to the free surface:

$$\begin{pmatrix} P_d+P_u \\ P_d-P_u \\ S_d-S_u \\ S_d+S_u \end{pmatrix} = \mathbf{E}_n^{-1} * \mathbf{A}\begin{pmatrix} u \\ w \\ 0 \\ 0 \end{pmatrix}.$$

We compute the differences, line 1 minus line 2 and line 3 minus line 4, of this equation:

$$\begin{pmatrix} 2P \\ -2S \end{pmatrix} = \mathbf{D}_1\begin{pmatrix} u \\ w \end{pmatrix}, \tag{8}$$

where $\mathbf{D}_1$ contains the first four elements of the difference matrix of $\mathbf{E}_n^{-1} * \mathbf{A}$. Equation (8) can now be used to compute the surface displacements u and w directly.

In summary, we use Eqs. (6), (4) and (3) to obtain the down-going P and S potentials at the source side. These potentials are used together with Eqs. (7) and (4) to compute the mantle-reflected, up-going potentials. These up-going potentials are used with Eq. (8) to compute the displacements at the free surface. The complete response is computed in each of these three parts of our model. We have introduced an artificial interface, which allows only down-going potentials at the source side and only up-going potentials at the receiver side. Multiple reflections through this interface are not included. Surface waves or phases like PP are therefore

not contained in our results. But the *P*- and *S*-wave groups are complete, provided the artificial interface is chosen properly. This method could also be used for studies of crustal structure, where different structures for the upper crust are needed.

Examples of application

Some recent examples of the application of theoretical seismograms to broadband data will be shown in the following. In particular, the new possibilities of the most recent extension of the method, derived in the previous sections, will be demonstrated in comparison with the older version of the method.

A) Swabian Jura

The Swabian Jura, the most active seismic zone in Germany, is the region with relatively strong events closest to the Gräfenberg array. For that reason the Swabian Jura events are very suitable for a demonstration of the usefulness of high-quality broadband recordings of local or regional earthquakes. The highest frequencies contained in the Gräfenberg data are 5 Hz and it is usually assumed that this frequency cut-off is not sufficient for studies of local earthquakes. This is certainly true for many problems but, on the other hand, it can be shown that frequencies below 5 Hz can contribute much new information if the stronger earthquakes are recorded in a suitable way.

Figure 1 shows the vertical and rotated radial and transverse components of the Gräfenberg station A1 of the Swabian Jura event of September 3, 1978 ($M_l = 6.0$) south of Stuttgart. The traces are proportional to ground displacement. The *P*-wave group is shown. The surface reflection of P_n, sP_n, was identified by Kind (1979b). This phase has also been identified by Zonno and Kind (1984) in Gräfenberg records of north Italian (mainly Friuli) earthquakes. A description of the sP_n phase is given there.

Note the phase shift between vertical and radial components in Fig. 1. This is an indication of a circular polarization instead of the expected linear polarization of the *P*-wave group (Axel Plesinger, personal communication). Its origin is not yet known. The observation of such a phase shift is difficult in analog data, and it is also not easy to observe if filters other than the simulation of a displacement record are used. The insufficient quality of older data is certainly the reason why these observations have not been made earlier. The modelling of these data will very likely lead to new information about the earth.

Figure 2 shows summation traces of a number of events from the Swabian Jura. All of the aftershocks of the large event of September 1978 also have the sP_n phase. This observation allows an accurate depth estimation of the main shock and the aftershocks. The deduction from this observation is that the rupture started with the main shock at about 6.5 km depth and the largest aftershocks migrated continuously within 5 h to a depth 2–3 km. The presence of sP_n in the data allows a direct observation of the time-dependent behaviour of the source depth. This migration of the aftershocks was not observed clearly by the usual methods of determination of hypocentres using a local network of stations (Turnowsky and Schneider, 1982).

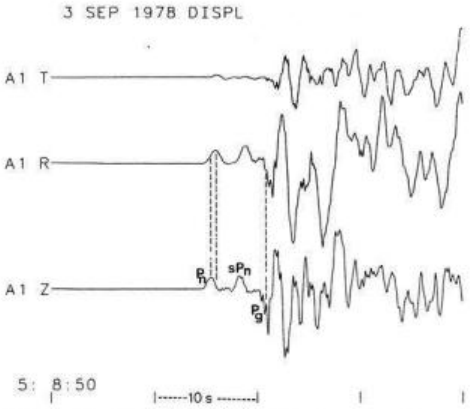

Fig. 1. Vertical, radial and transverse components of the Swabian Jura event of September 3, 1978, recorded at the Gräfenberg station A1 (epicentral distance 210 km). The *P*-wave group is shown, proportional to displacement. sP_n is a surface reflection of the P_n wave. Note the phase shift between vertical and radial components

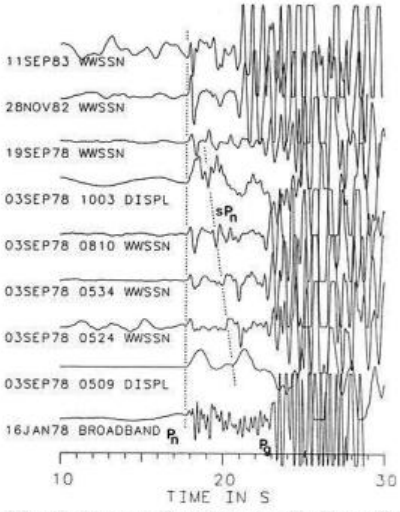

Fig. 2. Summation traces of all available vertical components for several Swabian Jura events. Different filters have been used in order to optimize the signal-to-noise ratio. The time difference between sP_n and P_n is an indication of the source depth. The aftershocks of the large event of September 3 at 0509 migrated within 5 h from 6.5 km depth to about 2–3 km depth

For comparison and phase identification, theoretical seismograms have been computed using the method developed above and the old method of Kind (1978, 1979a). Figure 3 shows a section of seismograms computed with the old method. The assumed model consists of a 30 km-thick crust with a *P* velocity of 6 km/s and a homogeneous mantle with a *P* velocity of 8 km/s. The shear velocity used was obtained by dividing the *P* velocity by the square root of 3. This is the simplest possible model. It was used because such a model produces relatively few phases and this makes the phase identification in the theoretical seismograms easier. The recording system in Fig. 1 was simulated. The typical

strike-slip orientation of the seismic sources of the Swabian Jura was used for the computation of the theoretical seismograms. The source-time function of Brüstle and Müller (1983) with a rise time of 0.5 s was used. This rise time is shorter than the observed pulse duration of P_n in Fig. 1, but the different phases are better separated for demonstrational purposes. P_n, sP_n and P_g are reproduced in the theoretical seismograms, although the signal shape does not fit the observed seismograms in Fig. 1 very well. No attempt has been made, so far, to improve the similarity. A more realistic crustal model could improve the similarity. Note, in particular, that the sign of P_g seems negative in the observed data in Fig. 1 and it is positive in the theoretical data in Fig. 3. Probably lateral heterogeneities in the crust have strongly modified the waveform of P_g. A comparison of the P_g onsets of all vertical array traces of the large Swabian Jura event indicates that P_g is a very emergent arrival and the sign is therefore unclear. The wave-forms and arrival times of P_g are also not very stable across the array.

Theoretical seismograms computed with the method developed in the previous section are shown in Fig. 4. The source and receiver structures were the same and all phases going directly from the source to the receiver are not computed by the method (like P_g and related phases). P_n, sP_n, PP and sPP are practically identical and P_g is gone. Also, a weak phase parallel to P_g is gone, which has travelled as a shear wave to the surface and from there as a converted P wave to the receiver. In this case the new method was used for phase identifications. Of course, phases in theoretical seismograms computed with the reflectivity method can be identified by simpler methods, but the method applied here can be useful in very complicated models where other methods could have problems. The waves travelling through the artificial interface could be controlled by setting arbitrarily up- or down-going P or S potentials equal to zero, respectively. That means one now has full control over up- and down-going P and S potentials in the reflectivity method, similarly to the equivalent possibility in Kennett's (1983) algorithm. The comparison Fig. 3 and Fig. 4 also proves that the new method is performing properly.

Figure 5 shows the theoretical seismograms as a function of the source depth for a fixed distance of 210 km. All depth phases can immediately be recognized in this figure.

The comparison between broadband records of regional earthquakes and theoretical seismograms has resulted in the identification of the depth phase sP_n in all the stronger Swabian Jura events (see observed data in Fig. 2 and theoretical data in Fig. 5). This interpretation is practically unique: the phase called sP_n cannot be a structural phase because its time difference to P_n varies from event to event; and it is probably not a second shock because it seems unlikely that most larger Swabian Jura events are double shocks. Theoretical seismograms for the most simple crust-mantle model, and the typical source orientation of the Swabian Jura events, model the observed phase as sP_n without contradiction provided the suitable source depth is chosen. These results clearly demonstrate the usefulness of digital broadband data for recording regional earthquakes, even if the highest frequencies are not recorded. The old version of the reflectivity method, without different source and receiver structures was, in this case, sufficient for the interpretation of sP_n. The existing lateral inhomogeneities between the Swabian Jura and the Gräfenberg array are not very important in this case. The new version of the reflectivity method has

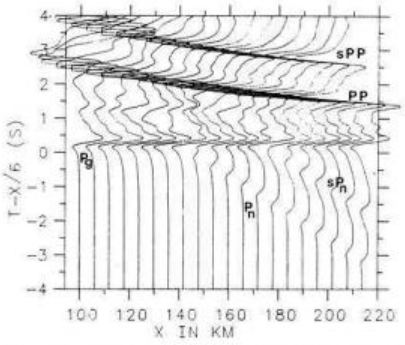

Fig. 3. Seismogram section of theoretical seismograms for the Swabian Jura event. The traces are proportional to displacement. PP is the Moho reflection. sPP is also a Moho reflection which has been reflected from the free surface beforehand. The model consists of a homogeneous crust and mantle (P velocity in the crust is 6 km/s, in the mantle 8 km/s, crustal thickness is 30 km)

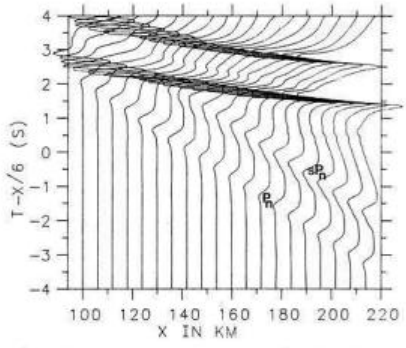

Fig. 4. The same theoretical seismograms as in Fig. 3 but computed with the method developed in this paper. The source and receiver structures are identical. Phases travelling directly to the receiver are omitted by this method (for example, P_g)

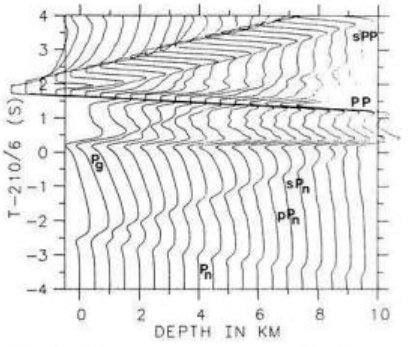

Fig. 5. The same theoretical seismograms as in Fig. 3, but at a fixed distance of 210 km and as a function of the source depth. It is very easy to identify all depth phases in this figure

been used in this section only for experimental purposes.

B) Aleutians

The first comparison of theoretical seismograms computed with the new extension and observed data was carried out with GRF records of earthquakes from the Aleutians. The source region near the Aleutians is covered by ocean, and this is not the case at the location of the Gräfenberg array. It is obvious that for a useful comparison with theoretical seismograms a method is required which takes these differences into account. It is especially interesting to see, in the case of an ocean-covered source region, what the influence of the ocean on the depth pP and sP is. The contrast of the material properties at the ocean bottom is very strong. Depth phases reflected at the ocean bottom and at the free surface have been observed by many authors (see, for example, Engdahl and Kind, 1985). It is also very interesting to compute, in addition to the reflections at the ocean bottom and at the free surface, the complete interaction of the wave field emitted by the source with the complicated earth structure near the source. All interfaces cause reflections and conversions and those near the source, especially, contribute to a complication of the source signal. It is very important for studies of the rupture process of an earthquake to have full control over the propagation effects. The new extension of the reflectivity method takes the layered structure near the source completely into account, independently of the structure at the receiver side. It allows numerical experiments with modifications of the source structure, keeping the receiver side fixed. However three-dimensional source structures cannot be considered, as usual in the reflectivity method. This is still a severe limitation of realistic modelling of observed data, since most hypocentres are located in complicated three-dimensional structures like subduction zones. Therefore the present extension of the reflectivity method still only allows a crude approximation of the real world, altough it is more complete than earlier similar methods.

The bottom trace of Fig. 6 shows the P-wave group of the event of July 13, 1981 in the Aleutians ($m_b = 5.5$) recorded at the array station A2. A displacement proportional record was simulated in Fig. 6, and the same is shown in Fig. 7 for WWSSN long-period simulation. Theoretical seismograms computed with the new method are also shown. They are computed for the case with (trace a) and without (trace b) a water layer on top of the source structure. The source depth is 16 km. The area is covered with a 5-km-thick layer of water, followed by a 1-km layer with a velocity of 5.2 km/s and a 4-km-thick layer with a velocity of 6.3 km/s. The structure at the receiver side is a simplified model of the crust underneath Gräfenberg. It consists of a 2-km-thick layer with a P velocity of 3.5 km/s and a 28-km-thick layer with a P velocity of 6 km/s. The P velocity at the top of the mantle is 8 km/s. The shear velocities are obtained by dividing the compressional velocities by the square root of 3. The water layer at the epicentre is approximated by a solid layer with a shear velocity of 0.01 km/s for the computation of theoretical

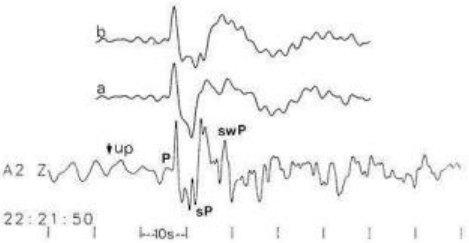

Fig. 6. *Bottom trace:* P-wave group of the event on July 13, 1981 in the Aleutians ($m_b = 5.5$, depth 16 km, epicentral distance 79°), proportional to displacement. sP is the reflection from the bottom of the ocean and swP is the reflection from the water surface which travelled through the ocean as a converted P wave. The traces above show theoretical seismograms computed with the new method. *Trace a* is for the model of the source region including the water layer. In *trace b* the water layer is replaced by a solid layer. sP is shifted to a later time in that trace. The polarity (arrow) is plotted in this unusual way because most events from the Aleutians have a similar source orientation, but reversed polarity (Engdahl and Kind, 1985)

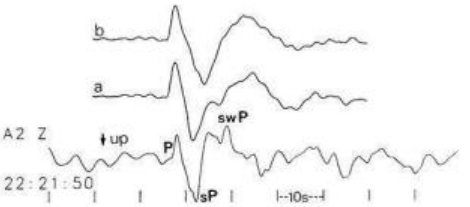

Fig. 7. The same as in Fig. 6 for the long-period WWSSN response

seismograms. The mantle in the epicentral region lies at a depth of 10 km below the ocean surface. The velocity structures at the Aleutians are taken from local studies (Engdahl and Kind, 1985). The Jeffreys-Bullen mantle model was used and the artificial interface required by the method is at 100 km depth. The orientation of the fault plane is: strike = 70°, dip = 50° to the north-west and slip = −90° (Engdahl and Kind, 1985). The azimuth to Gräfenberg is 357° from the epicentre. A frequency window from zero to 2.9 Hz and a rise time of 1 s in the source-time function of Brüstle and Müller (1983) was used in the computations. This rise time results in a corner frequency of 1.1 Hz. This high-frequency cut-off was not large enough, compared with the observed data, but it has been used in order to save computer time. The computer time was 12 h on a VAX 780 for computing the theoretical seismograms in Fig. 6 and 7. The slowness integration was carried out in a window corresponding to the apparent velocities between 9 and 19 km/s. There is some numerical noise in front of the first onset, especially in the theoretical seismograms in Fig. 6. These are numerical phases related to the fast limit of the slowness integration. They are typical for the reflectivity method. They can be suppressed by applying a taper at the end of the slowness window. The equivalent phenomenon in the case of the Fourier transformation is ringing in the time domain, if the cut-off in the frequency domain is too steep. No taper was used in the slowness integration for computing Figs. 6 and 7.

The phase marked sP in these figures is the reflection from the bottom of the ocean and the phase marked swP is the surface reflection which travelled as a converted P wave through the ocean. The surface reflections pP and pwP arrive, because of the small source depth, only slightly earlier than sP and swP and they are weaker and not clearly separated from these two phases (Engdahl and Kind, 1985). sP has shifted to a later time in the case where the water layer is replaced by a solid layer with a velocity of 5.2 km/s, because it is now the usual reflection from the surface of the earth which is located further from the source than the ocean bottom. The artificial layering, used for the approximation of gradients, has been chosen very fine so that the theoretical seismograms are not much influenced by that approximation. It is interesting to see that the WWSSN simulation of the theoretical seismograms for the two models with and without water are significantly different at the first minimum of the trace. Depth phases are contributing strongly to this minimum.

The general agreement between the observed bottom trace, especially in the long-period data in Fig. 7, and the computed trace a seems to be fairly good. In detail, however, there are still many things which could be improved. Modifications of the source depth or the structure near the source would have the largest influence on the signal form of the entire P-wave group. The long-period part following swP, especially, could be brought to better agreement by such means. But we cannot hope to achieve very close agreement because there are still many parameters which influence the waveform in the real earth and over which we have no control. Another question is how representative the record at a single site is for a larger area, or how important very local effects of the receiver site are. This problem can be treated by using averaged records over all the Gräfenberg traces. Then undesired site effects will be reduced.

Conclusions

The main purpose of this paper was to derive a version of the reflectivity method which allows the computation (in most parts of the model) of complete theoretical seismograms for different source and receiver structures. This has been achieved, and first comparisons with observations have been carried out. It was shown that the new method performs well. It was not the purpose of this paper to show definitive new results of data interpretation. Rather, it was intended to illustrate examples of how theoretical seismograms might be applied. Nevertheless, the examples from the Swabian Jura events clearly demonstrate the usefulness of broadband data for the interpretation of regional earthquakes. They permit the interpretation of details of the waveform which, so far, could not be seen.

References

Brüstle, W., Müller, G.: Moment and duration of shallow earthquakes from Love-wave modeling for regional distances. Phys. Earth Planet. Inter. **32**, 312–324 1983

Chang-Eob Baag, Langston, Ch.A.: A WKBJ spectral method for computation of SV synthetic seismograms in a cylindrically symmetric medium. Geophys. J.R. Astron. Soc. **80**, 387–417, 1985

Dunkin, J.W.: Computation of modal solutions in layered media at high frequencies. Bull. Seismol. Soc. Am. **55** (2), 335–358, 1965

Engdahl, E.R., Kind, R.: Interpretation of broadband seismograms from central Aleutian earthquakes. Ann. Geophys., in press, 1985

Fuchs, K.: The reflection of spherical waves from transition zones with arbitrary depth-dependent elastic moduli and density. J. Phys. Earth **16** (Special Issue), 27–41, 1968

Fuchs, K., Müller, G.: Computation of synthetic seismograms with the reflectivity method and comparison with observations. Geophys. J.R. Astron. Soc. **23**, 417–433, 1971

Harkrider, D.G.: Surface waves in multilayered elastic media. 1. Rayleigh and Love waves from buried sources in a multilayered elastic halfspace. Bull. Seismol. Soc. Am. **54**, 627–679, 1964

Kennett, B.L.N.: Theoretical seismograms for calculation of laterally varying crustal structures. Geophys. J.R. Astron. Soc. **42**, 579–589, 1975

Kennett, B.L.N.: Seismic wave propagation in stratified media. Cambridge University Press, 1983

Kind, R.: The reflectivity method for a buried source. J. Geophys. **44**, 603–612, 1978

Kind, R.: Extensions of the reflectivity method. J. Geophys. **45**, 373–380, 1979a

Kind, R.: Observations of sP_n from Swabian Alb earthquakes at the GRF array. J. Geophys. **45**, 337–340, 1979b

Kind, R., Odom, R.I.: Improvements to layer matrix methods. J. Geophys. **53**, 127–130, 1983

Phinney, R.A.: Theoretical calculation of the spectrum of first arrivals in layered elastic mediums. J. Geophys. Res. **20**, 5107–5123, 1965

Schwab, F.A., Knopoff, L.: Fast surface wave and free mode computations. In: Methods in Computational Physics, vol. II, B.A. Bolt, ed., New York: Academic Press 1972

Turnowsky, J., Schneider G.: The seismotectonic character of the September 3, 1978 Swabian Jura earthquake series. Tectonophysics **83**, 151–162, 1982

Zonno, G., Kind, R.: Depth determination of north Italian earthquakes using Gräfenberg data. Bull. Seismol. Soc. Am. **74**, (5), 1645–1659, 1984

Zurmühl, R.: Matrizen und ihre technischen Anwendungen. Springer Verlag 1964

Received January 24, 1985; revised version May 21, 1985
Accepted June 20, 1985